C. R. Mecanique 339 (2011) 443–457

Contents lists available at ScienceDirect

Comptes Rendus Mecanique

www.sciencedirect.com

Surface mechanics: facts and numerical models

Characterization of the adhesion of thin film by Cross-Sectional Nanoindentation
Analysis of the substrate edge chipping and the film delamination

Eric Felder *, Sébastien Roy, Evelyne Darque-Ceretti

CEMEF, UMR CNRS/MINES ParisTech 7635, BP 207, 06904 Sophia-Antipolis, France

ARTICLE INFO

Article history:
Available online 21 June 2011

Keywords:
Adhesion
Nanoindentation
Thin films
Microelectronic
Copper
Mechanical analysis

ABSTRACT

Cross-Sectional Nanoindentation (CSN) is a recent method for adhesion measurement of nanoscale thin films in Ultra-Large Scale Integrated circuits. In the case of ductile thin films, the motion of the substrate chip implies significant plastic deformation of the film and complex geometry of delaminated areas. This article recalls first the experimental procedure and the two main features observed in this test performed on various plane copper films deposited on silicon: the critical force producing silicon edge chipping increases linearly with the distance of the indenter to the interface; on the section the delaminated length of the film $(a-b)$ is proportional to the residual silicon chip displacement u_f and the ratio $S = u_f/(a-b)$ depends on the manufacturing process of the film, and is so related to its adhesion to the substrate. One proposes a simple analysis of the silicon edge chipping. Then a model of pull-off of an elastic-strain hardening plastic film is developed, which suggests an explanation for the delamination process. Application of the model to experimental results starting from films plastic properties deduced from nanoindentation measurements provides plausible results. Some improvements for performing the CSN test are proposed in order to make easier its interpretation.

© 2011 Académie des sciences. Published by Elsevier Masson SAS. All rights reserved.

1. Introduction

Due to its low electrical resistivity, copper (Cu) has been widely adopted for microelectronic interconnect structures in Ultra-Large Scale Integrated (ULSI) circuits. The reliability of electronic devices is strongly dependent on interfacial adhesion and mechanical properties of Cu thin films. Insufficient adhesion can lead to interfacial delamination during Chemical Mechanical Polishing (CMP) and to high electromigration failure rate of copper during device operation. Compared to aluminum, copper presents low adhesion with most of dielectric materials, therefore adhesion measurement became one of the most important challenges for process technology development.

There exist numerous mechanical tests used for measuring the strength of joinings [1,2], but very few simple techniques allow adhesion assessment of nanoscale films. It is very difficult to perform a peeling test [3] on very thin films; in addition, plastic deformation of the film occurs generally and the interpretation of the peeling force is not easy [1]. Producing the spontaneous peeling of the film by deposition of an additional film with high residual stress [4] is a very interesting test, but requires a deposition technique. The blister test [5] is also very attractive, but it needs micromachining of the substrate and precise control of the volume of injected liquid under the blister and measurement of its pressure. The four Point Bending test (4PB) [6,7] is currently the most used technique for adhesion measurement in microelectronics. This method

* Corresponding author.
E-mail address: Eric.Felder@mines-paristech.fr (E. Felder).

1631-0721/$ – see front matter © 2011 Académie des sciences. Published by Elsevier Masson SAS. All rights reserved.
doi:10.1016/j.crme.2011.05.003

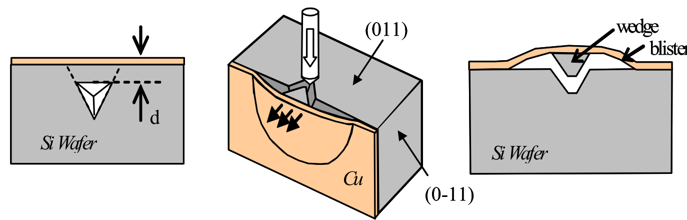

Fig. 1. CSN test configuration.

was recently applied to a polymer/SiO_2 patterned structure to measure the macroscopic adhesion of the interface and the influence of the aspect ratio of polymer lines [8]. However the 4PB test requires a complex sample preparation: a multi-stack of thin films must be produced and the samples have to be precisely pre-notched to ensure that the crack propagates at the interface of interest. Test interpretation is also difficult because the crack path is complex and must be studied by XPS analysis.

By using the model of the lateral crack system generated during indentation of semi-brittle solids, Chiang et al. [9] tried for the first time to propose a model of film delamination by macro or microindentation performed on rather thick films surface. This technique was investigated by many authors [1,10–12] notably for the characterization of the adhesion of hard brittle films deposited on softer tougher substrates. Instrumented nanoindentation has been recently employed for the adhesion measurement of nanoscale thin films [13–15]. The indentation force, applied normally to the surface, produces a delaminated blister whose dimensions are used to calculate adhesion. In the case of ductile coatings, like copper, deposition of a hard encapsulating layer with high residual stresses is necessary to promote the delamination. Crack localization, which is critical for interpretation, requires Focused Ion Beam (FIB) cross sectioning of the blister. Finally a very common technique for adhesion measurement of thin films is the scratch test performed at various forces and indenter size scales [16]. It is very useful and it is possible in some cases to correlate the delamination pattern extent in this test with that observed in indentation [17], but the mechanical analysis of the scratch test is very complex [1] and requires generally three-dimensional (3D) finite element calculations [18].

In parallel to this use of the indentation test at various scales, Lesage et al. [19] test the adhesion of thick coatings by performing Vickers microindentation on a cross section, a diagonal of the indenter being located along the interface: the adhesion is characterized by the evolution with the force of the length of the crack running along the interface. Cross-Sectional Nanoindentation (CSN), developed by Sanchez et al. [20], is a new technique to access Cu thin film adhesion on blanket and patterned structures. CSN was first employed for the study of adhesion between dielectric brittle thin films; therefore an analytical model based on the elasticity theory could be developed to calculate the interfacial critical energy release rate G_c for these elastic layers. For copper-dielectric adhesion measurement, a two-dimensional (2D) Finite Element Modeling (FEM) was used to take into account the plastic behavior of metal into G_c calculation [21]. Recently, the CSN test was also applied to patterned interconnect structures [22–24] to study crack propagation at complex interfaces.

One performed recently CSN tests on copper films deposited on silicon [18,25]. The edge chipping of the silicon and the delamination patterns are different from those observed or assumed in these previous works. A three-dimensional (3D) analysis has been developed as a tentative way for interpretation of the results. In this article one recalls the main observed features and proposes a simple mechanical analysis of the test in order to explain them.

2. Experimental approach and results

2.1. Samples and experimental procedure

The studied samples consist of electroplated (ECP) copper thin films deposited on a Ta/TaN/SiO_2 (or SiC)/Si substrate. The surface of the silicon corresponds to the (100) crystalline plane. A Ta (15 nm)/TaN (10 nm) stack is used as a barrier bilayer to avoid Cu diffusion in SiO_2. The ECP copper thickness is $h = 0.6$ µm. Three processes were used for Cu deposition: processes A, B and C, which are known to give, respectively, low, medium and high adhesion copper films. In addition one considers some experimental results related to other manufacturing routes (X1, X2, X3) in order to obtain confirmation of the conclusions.

First, samples are precisely cleaved through one crystalline plane of silicon substrate of the family (011) (Fig. 1) by pre-scratching one edge with a diamond. Cleaved surfaces are perfectly straight and have a mirror aspect. CSN experiments were performed on a Nano-Indenter® XP using a Berkovich indenter. Special sample holders were used to maintain cleaved samples in a vertical position during indentation. The indentation force is applied on the silicon substrate, normally to the cross-sectional plane, at a distance d from the interface of interest. One side of the Berkovich indenter must be parallel to the interface (Fig. 1). The indenter–interface distance d is chosen between 2 and 10 µm, but cannot be precisely controlled due to the lack of precision of the apparatus.

At a certain stage of the indentation process a crack starts in the silicon substrate at the two corners of the Berkovich indenter and then propagates through the weakest interface, inducing a small delaminated blister. The silicon fragment (wedge or chip) is removed from the substrate and remains stuck to the Cu film. In some cases, the crack propagates

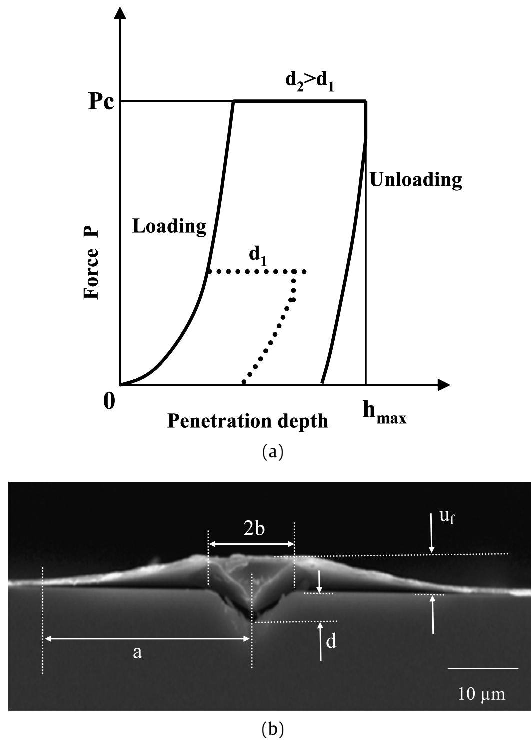

Fig. 2. Results of CSN test. (a) Schematic evolution of the force P with the penetration depth P of the indenter during CSN test. (b) SEM observation of CSN experiments on blanket substrate (process A: $U_f/(a-b) = 0.16$) and definition of the various geometrical quantities.

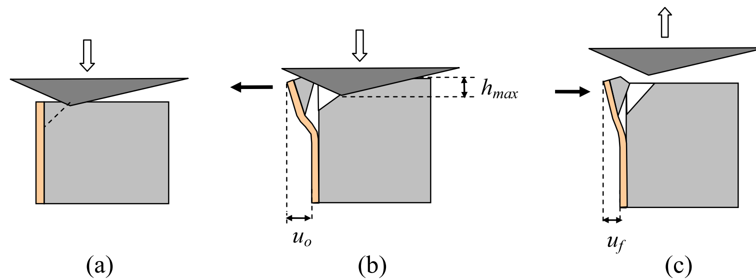

Fig. 3. Schematic description of the phenomena occurring during the CSN test: (a) penetration, (b) edge chipping of silicon and film delamination, (c) unloading and elastic recovery.

through the film and produces its ablation by shearing: in such circumstances the test provides no information on the adhesion of the film.

2.2. Edge chipping of the silicon

Fig. 2a shows the shape of the force–displacement curves observed for successful CSN experiments on different samples and with various distances d. In fact, according to the experimental results, only the distance d has a significant influence on these curves. The indenter–interface distance d is measured post-test by Scanning Electron Microscopy (SEM) (Fig. 2b). The crack initiates in the substrate at a critical load P_c and then we observe a step where the displacement increases before unloading occurs (Fig. 3). The maximal penetration depth for indentation, which is required in the test inputs, is usually fixed between 600 and 1000 nm. However, it cannot be precisely controlled due to fracture velocity and because the nanoindenter is load controlled. The effective maximal indenter displacement $h_{\max}$ is given by the magnitude of the step.

We can notice in Fig. 2a that the critical load P_c and the step amplitude increase with the indenter–interface distance d. High P_c results in high fracture velocity and so in high $h_{\max}$. Performing various tests at different locations and on different samples, we could notice that the data are repeatable.

As shown in Fig. 4, the critical load P_c increases linearly, in first approximation, with indenter–interface distance d and is not influenced by location of test on the sample or sample type. Some scatter remains, probably due to the brittle behavior of silicon crystal and to the defects induced by cleavage. The force P_c is mostly related to silicon toughness (see later) and

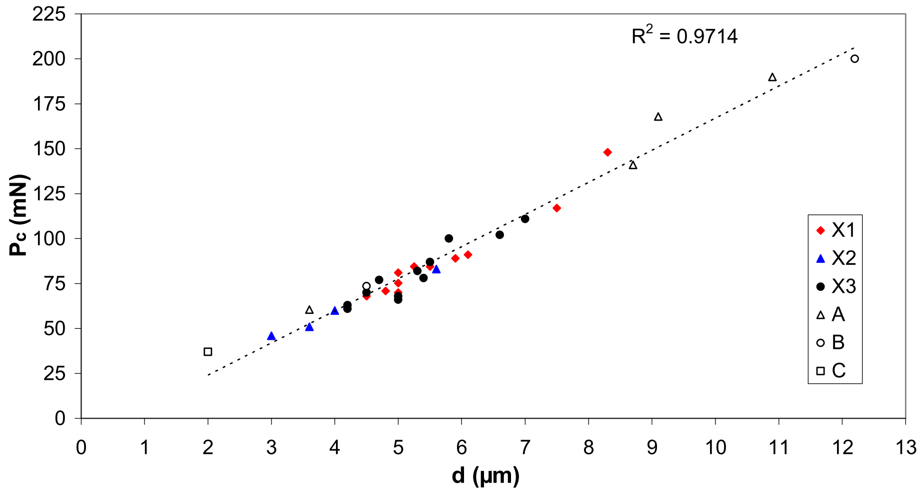

Fig. 4. Critical load P_c versus the indenter–interface distance d.

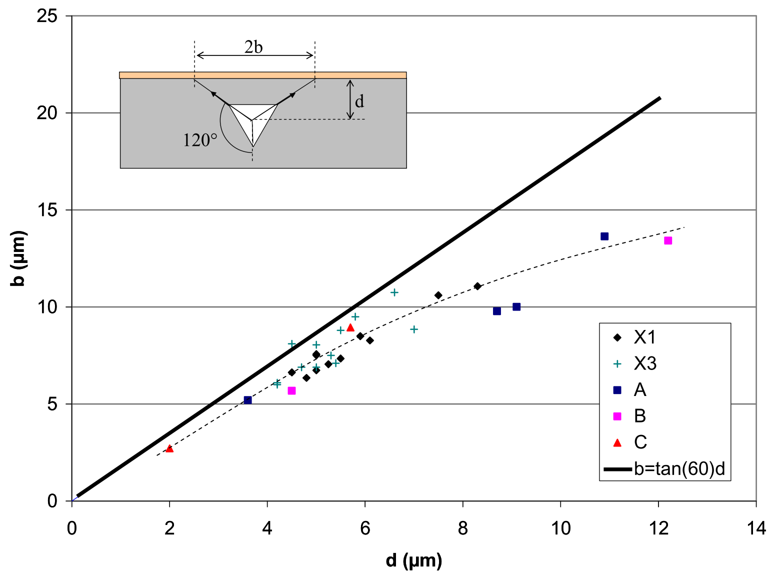

Fig. 5. Evolution of b with d for various CSN tests and comparison with simple relation $b = d\tan(60^\circ)$.

may not be influenced significantly by the copper adhesion or the mechanical properties of the films. A larger scatter is observed on step amplitude h_{max}. The maximal penetration of the indenter is very difficult to control during this very quick fracture process.

Fig. 2b defines the various geometrical quantities characterizing the final geometry in the cross-sectional plane: the chip width $2b$, its residual displacement u_f and the semi-length of the delaminated blister a. Fig. 5 describes the evolution of the semi-width b of the silicon chip versus the distance to the interface d which is equal to its height as revealed by SEM observations [18,25]. One sees that the crack does not propagate exactly along the direction of the indenter diagonals as revealed by the gap between the experimental values and the plain line. In addition the highest values suggest an evolution of the relation between b and d.

2.3. Film delamination process

The maximal indenter displacement, h_{max}, gives the maximal residual wedge displacement u_f, but with some significant scatter (Fig. 6) due probably to this uncontrolled rupture process. If the wedge displacement is too high because d is too high, the CSN test can lead to the rupture of the Cu film. One possible explanation is that the angle between the interface and the crack running in the silicon changes with d: so for high d the bifurcation angle of the crack as it passes along the interface increases with d and prevents its bifurcation for high d. One notices in Fig. 6 that the residual chip displacement

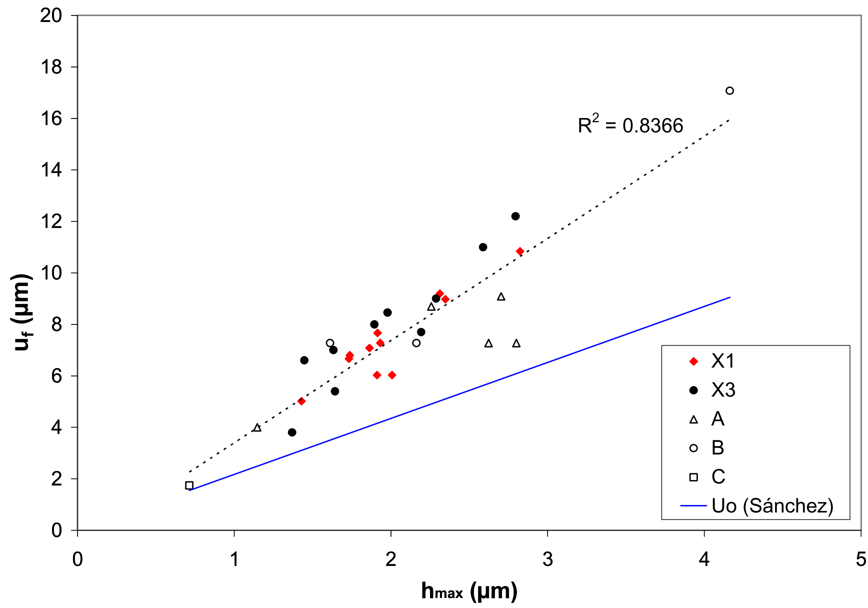

Fig. 6. Evolution of the residual displacement of the silicon chip U_f versus the maximal penetration depth of the indenter $h_{\max}$ and comparison with the model of Sánchez et al. [20].

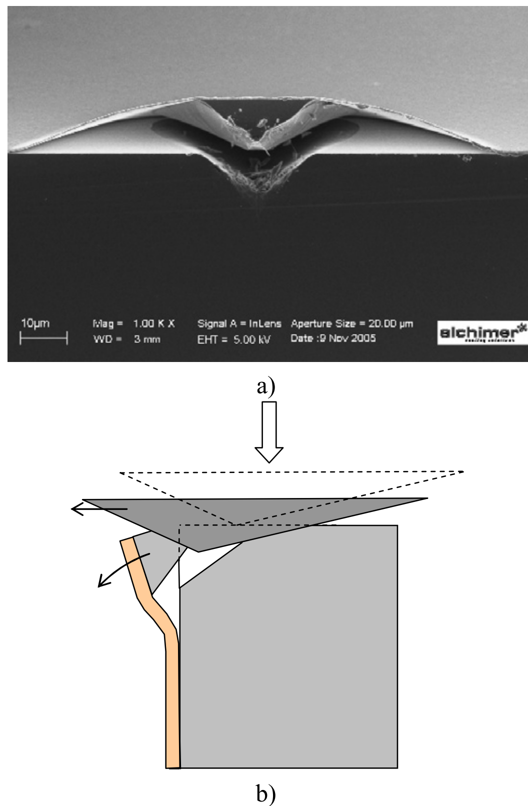

Fig. 7. (a) SEM tilted view of a CSN test. (b) Probable motion of the silicon chip during the film delamination.

is higher than the displacement estimated previously by assuming that the motion of the chip is a translation normal to the initial surface of the sample. It suggests that this motion is more complex and involves some rotation of the chip (Fig. 7).

Fig. 8a provides the evolution of the crack length $(a - b)$ versus the wedge displacement u_f for various tests on samples with processes A, B and C. We can notice that $(a - b)$ is proportional to u_f for each sample. The slope of the curve

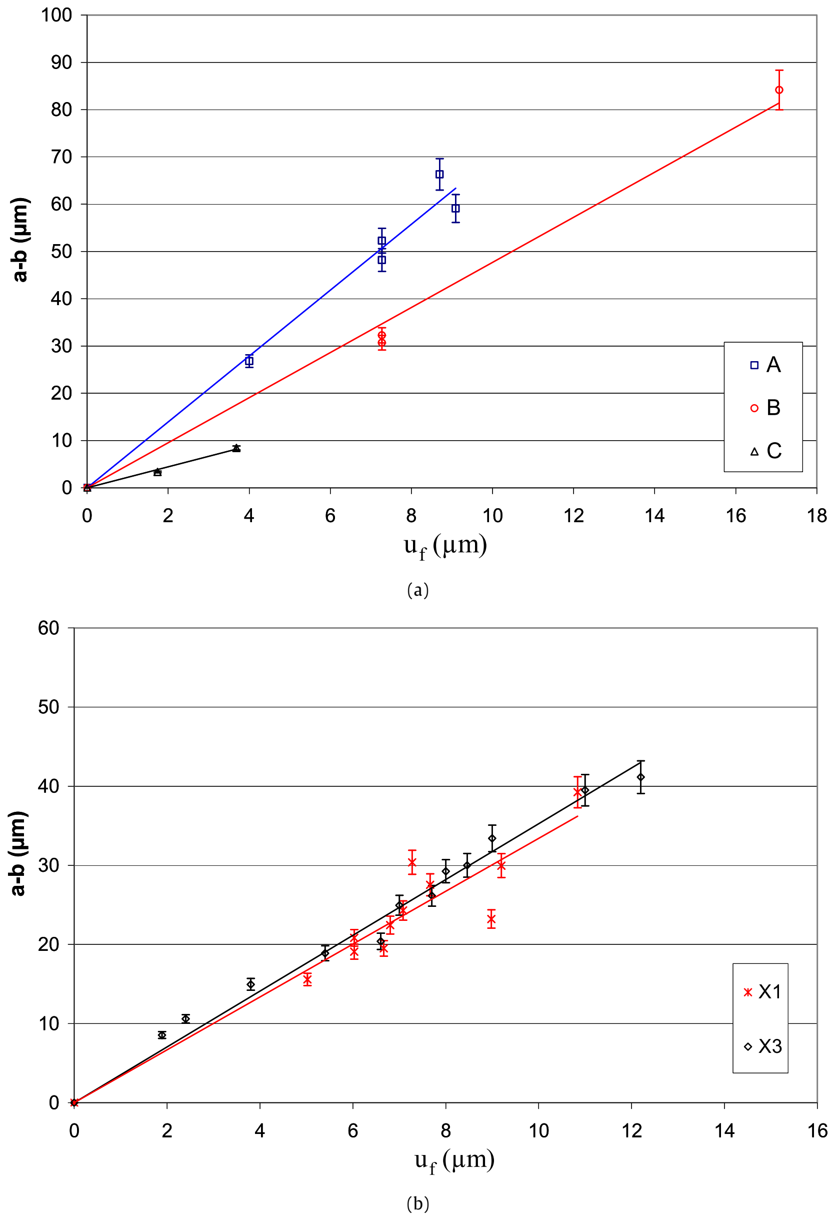

Fig. 8. Blister dimensions (crack length $(a-b)$ vs. wedge displacement u_f) for various CSN tests for samples manufactured with (a) processes A, B, C and (b) processes X1, X3.

decreases with adhesion enhancement. There are rather few points in Fig. 8a, but the linear evolution of $(a-b)$ versus u_f is confirmed with more numerous tests performed on samples elaborated by routes X1, X2 and X3. For the same film thickness and mechanical properties, adhesion can then be evaluated using the geometrical ratio of blister dimensions:

$$S = \frac{u_f}{a-b} \tag{1}$$

High adhesion results in high S ratio and vice versa. Average ratio S is 0.144 for samples with process A, 0.22 for process B and 0.47 for process C. The spread is of about 5% due to the dimensions measurement error.

The crack can be directly observed and precisely localized using both secondary (SE) and back-scattering electron (BSE) imaging without post-test treatments. Three main crack paths have been observed depending on the adhesion of copper:

- For samples with processes A and B, which have the lowest adhesions, the debonded interface is Cu/Ta;
- On the other hand, for samples with process C, which have the highest adhesion, SEM observations show that the delaminated interface is TaN/SiO_2. These results demonstrate that process C results in a very strong Cu/Ta interface;

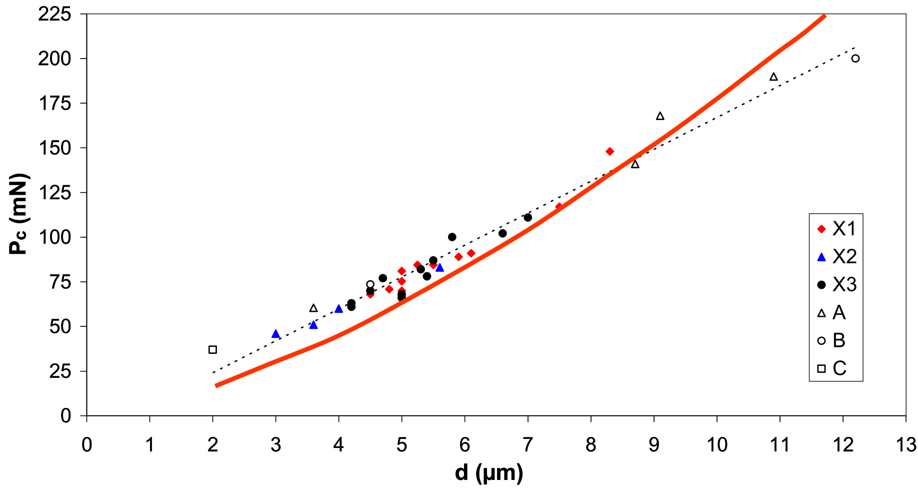

Fig. 9. Test of edge chipping model of Chai and Lawn: the curve is the relation (2) with $K_c = 0.6$ MPa m$^{1/2}$.

- A third type of crack path, which was frequently observed on sample with process C, and when distance d is too high, is propagation of the crack thought Cu layer and tearing of the film. In this case, the adhesion cannot be calculated. Like other techniques, the CSN test does not provide results when the adhesion is too high [1].

3. Analysis of the substrate rupture

3.1. Application of current model

The formation of the silicon chip is similar to the edge chipping studied by Chai and Lawn [26] by Vickers indentation in zirconia, alumina, porcelain and glass. However, the distance d between the indenter and the surface is much greater and ranges between 0.2 and 2 mm. One diagonal of the indenter was parallel to the surface and forces higher than 1 N were progressively applied. They observed the formation of four radial/median cracks at the edges of the prints; their lengths increase in a stable manner with the force and progressively the length of the two cracks related to the diagonal parallel to the surface becomes greater and they deviate toward the surface till a critical force P_c where edge chipping occurs. They demonstrate that the critical force is related to the distance d and the toughness K_c of the material by the relation:

$$P_c = 9.3 K_c d^{3/2} \tag{2}$$

The constant 9.3 has been chosen in order to provide the best fitting of the experimental results. One compares in Fig. 9 our experimental results to the values provided by this relation by taking $K_c = 0.6$ MPa m$^{1/2}$. The order of magnitude is good, but the shape of the curve is not in very good agreement with the general trend of the experimental values.

This relative discrepancy cannot be explained by the choice of the value of the silicon toughness. Values provided by papers [27,28] are rather scattered. For example, the cracking behavior of crystalline silicon induced by Berkovich indenter suggests a value $K_c = 0.9$–1.25 MPa m$^{1/2}$. But first this value is related to indentations performed on the (100) plane; then one can remark that if one increases (decreases) K_c, the gap increases for high (small) values of d.

One must notice that the indenter geometry and especially the initial direction of the generated cracks are different: in our experiments performed with Berkovich pyramid, the cracks run as soon as they are formed toward the interface, whereas for Vickers indentations they deviate toward the surface when the stress field is perturbed by the surface. These points would require further work and probably 3D numerical calculations. At present time one tries below to propose a better model. However, let us recall simple relations useful for this. First one has for a material with Young's modulus E the classical relation between its toughness and its critical energy release rate G_c or rupture energy [1]:

$$G_c \approx \frac{K_c^2}{E} \tag{3}$$

During conical indentation of a material with hardness H, the (equivalent for pyramid) contact radius a and the radial stress σ at a radial distance r from the indenter tip are:

$$a = \sqrt{\frac{P}{\pi H}} \quad \text{and} \quad \sigma(r \geqslant a) \sim \frac{P}{\pi r^2} \tag{4}$$

3.2. Theoretical model

One possible explanation for this discrepancy is that our experiments are performed with small d values and thus for forces P near the cracking threshold force P^* [27–29]: according to these papers, for silicon $P^* \sim 20$–40 mN. So edge chipping occurs when the cracks are not well developed. In order to test our method of approach let us first consider the evaluation of P^* and the steady state increase of a well developed radial crack of length c.

3.2.1. Cracking threshold force P^*

At the cracking threshold force P^*, a fraction of the elastic energy stored in the core and just around the print (stress $\sim$ hardness H, volume $\sim a^{*3}$) is released for forming a crack surface area $\sim a^{*2}$. So:

$$\frac{1}{2}\frac{H^2}{E}a^{*3} \sim \alpha G_c a^{*2} \tag{5}$$

α is some numerical constant (as $\alpha', \beta, \beta', \gamma$ and γ' later). Thus, with the relation (3) and the first relation (4), one obtains the classical relation [29]:

$$P^* \sim \alpha' \frac{K_c^4}{H^3} \tag{6}$$

3.2.2. Expansion of a well-formed half-penny crack

As the radius c of the crack increases by dc, a fraction of the elastic energy stored in the volume located between the radial distance c and $c + \mathrm{d}c$ is released for increasing the crack surface area of $c\,\mathrm{d}c$. So:

$$\frac{1}{2}\frac{\sigma^2(c)}{E}\pi c^2\,\mathrm{d}c \sim \beta G_c 2\pi c\,\mathrm{d}c \tag{7}$$

By using the relation (3) and the second relation (4), one obtains the classical relation [30,31]:

$$P = \beta' K_c c^{3/2} \tag{8}$$

Notice that this relation is the basis of the relation (2) [26].

3.2.3. Edge chipping for $P < P^*$

One assumes that the edge chipping occurs suddenly by release of the elastic energy stored in the volume located between the radial distance a and d for forming a crack surface $\sim d^2$. So:

$$\frac{1}{2E}\int_a^d \sigma^2(\mathrm{r})\pi r^2\,\mathrm{dr} \sim \gamma G_c \pi d^2 \tag{9}$$

By using the relation (3) and the relations (4), one obtains the implicit relation between P_c and d:

$$\frac{P_c}{d}\left(\sqrt{\frac{\pi H}{P_c}} - \frac{1}{d}\right)^{1/2} = \gamma' K_c \tag{10}$$

In Fig. 10 are plotted the experimental values and the values deduced from this relation for $H = 10$ GPa and a value $\gamma' = 15.8$ which gives the best fit for $K_c = 0.6$ MPa m$^{1/2}$. Evidently it is only the product of these two quantities which is important. One observes that the agreement is better than in Fig. 9. Indeed, further work is required. In particular, one can expect that for higher values of d and P_c, the relation (2) must be recovered and this requires one to improve this simple model.

4. Analysis of film delamination

SEM observations show that the debonding process induces a very large plastic deformation of the Cu film. The plastic energy dissipation must be considered for adhesion quantification. In [18,25] one tries to simulate this deformation process by 3D finite element calculations, but this approach presents some difficulties: first it is difficult to know the real conditions during the delamination process and some simplifying assumptions have been made. Most importantly, this work does not provide an explanation of the main experimental result: the delaminated length $b - a$ increases in direct relation with the residual central displacement U_f (Fig. 8). So one proposes a model which is a generalization of the model of elastic film pull-off developed by Gent [32].

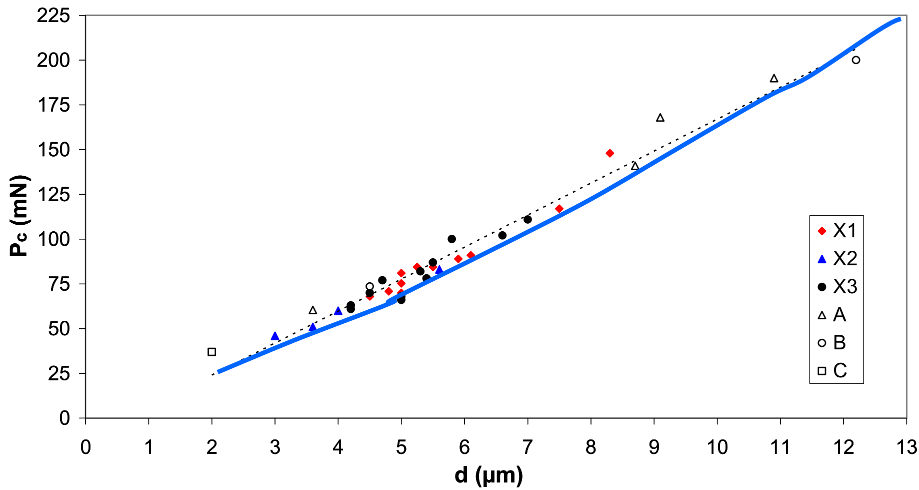

Fig. 10. Test of the present model of edge chipping (theoretical curve for $\gamma' = 15.8$ and $K_c = 0.6\ \text{MPa}\,\text{m}^{1/2}$).

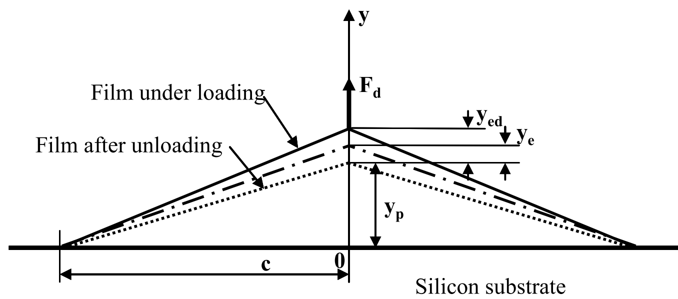

Fig. 11. Model of the film delamination: elastic–plastic pull-off test of the film.

4.1. Model of deformation of the film

One neglects the strain in silicon during the delamination process. Fig. 11 describes schematically the model: One assumes that the silicon block extends the film which is submitted at each time to an uniaxial stress σ_d. Each slab of the film parallel to the cross-sectional plane is submitted to the same strain and stress, simply the delaminated length and the chip displacement decreases from the cross section to 0 at the chip depth (2b). The Young's modulus and the Poisson's ratio of the film are E and υ. At a given time, a section of the film is delaminated on a length $2c$ under the action of a vertical force F_d (per unit film width) after a displacement y (Fig. 11).

Due to the elasticity of the film, during unloading, the displacement decreases to y_p. For a partial recovery, one has:

$$y = y_p + y_e \tag{11}$$

One assumes that the elastic displacement remains small with respect to c. So the plastic and elastic strains during partial unloading are given by the elementary geometrical relations:

$$\varepsilon_p = \ln\sqrt{1 + \frac{y_p^2}{c^2}}, \qquad \varepsilon_e = \sqrt{\frac{c^2 + (y_p + y_e)^2}{c^2 + y_p^2}} - 1 \sim \frac{y_p y_e + y_e^2/2}{c^2 + y_p^2} \tag{12}$$

As we shall see below some strain hardening occurs in the films. So one assumes that their uniaxial flow stress σ_0 is described by the classical Hollomon relation:

$$\sigma_0 = \sigma_1 \varepsilon_p^n \tag{13}$$

One assumes that the film extends under plane strain. So it is interesting to introduce the representative modulus and strength (for von Mises yield criterion) [33]:

$$E^* = \frac{E}{(1 - \upsilon^2)}, \qquad \sigma_1' = \frac{2}{\sqrt{3}}\sigma_1 \tag{14}$$

During the delamination process, the stress σ_d in the film verifies the yield criterion and the elasticity relation. So:

$$\sigma_d = E^* \varepsilon_{ed} = \sigma_1' \varepsilon_p^n \quad \Rightarrow \quad \frac{y_p y_{ed} + y_{ed}^2/2}{c^2 + y_p^2} = \frac{\sigma_1'}{E^*} \varepsilon_p^n \tag{15}$$

In fact, for $n \neq 0$, this equation implies that some plastic strain occurs for all values of y, but as y increases, y_e becomes small with respect to y_p. So one shall simplify some formulae by neglecting y_e with respect to y_p. For an analysis of the problem one applies the thermodynamic approach of adherence. The second principle of thermodynamics reads [1]:

$$F \frac{\mathrm{d}y}{\mathrm{d}t} - \frac{\mathrm{d}V}{\mathrm{d}t} \geqslant 0 \tag{16}$$

V is the variable free energy of the system, sum of the interface free energy and the elastic energy of the film. By neglecting the volume change of the film due to its elastic strain, one has:

$$V(y_e, y_p, c) = \frac{E^*}{2} 2ch\varepsilon_e^2 + 2wc = E^* h \frac{c(y_p y_e + y_e^2/2)^2}{(c^2 + y_p^2)^2} + 2wc \tag{17}$$

w is the Dupré's work of adhesion of the film to the substrate [1]. By taking into account the relation (11):

$$F \frac{\mathrm{d}y}{\mathrm{d}t} - \frac{\mathrm{d}V}{\mathrm{d}t} = F \frac{\mathrm{d}y_e}{\mathrm{d}t} + F \frac{\mathrm{d}y_p}{\mathrm{d}t} - \frac{\partial V}{\partial y_e} \frac{\mathrm{d}y_e}{\mathrm{d}t} - \frac{\partial V}{\partial y_p} \frac{\mathrm{d}y_p}{\mathrm{d}t} - \frac{\partial V}{\partial c} \frac{\mathrm{d}c}{\mathrm{d}t}$$

$$\text{So} \quad \left(F - \frac{\partial V}{\partial y_e}\right) \frac{\mathrm{d}y_e}{\mathrm{d}t} - \frac{\partial V}{\partial (2c)} \frac{\mathrm{d}(2c)}{\mathrm{d}t} + \left(F - \frac{\partial V}{\partial y_p}\right) \frac{\mathrm{d}y_p}{\mathrm{d}t} \geqslant 0 \tag{18}$$

For each irreversible (reversible) process induced by the increase of a state variable, the related term in the previous relation is positive (zero). As y_e is related to the reversible elastic deformation of the film, we have:

$$F = \frac{\partial V}{\partial y_e} = 2E^* h \frac{c(y_p y_e + y_e^2/2)(y_p + y_e)}{(c^2 + y_p^2)^2} \tag{19}$$

So according to the relation (15), the delamination force is:

$$F_d = 2\sigma_1' h \frac{(y_p + y_{ed})/c}{1 + (y_p/c)^2} \varepsilon_p^n \tag{20}$$

The second term of (18) defines the energy release rate G and, according to previous relations, its critical value is obtained for $\varepsilon_e = \varepsilon_{ed}$:

$$G = \frac{\partial V}{\partial (2c)} + w = \frac{E^* h}{2} \left(\frac{4c^2}{c^2 + y_p^2} - 1\right) \left[\frac{y_p y_e + y_e^2/2}{c^2 + y_p^2}\right]^2 \quad \Rightarrow \quad G_c = G(y_{ed}) = \frac{h\sigma_1'^2}{2E^*} \left(\frac{4}{1 + (y_p/c)^2} - 1\right) \varepsilon_p^{2n} \tag{21}$$

The energy release rate depends on the mechanical properties of the film and on the ratio y_p/c. As this ratio increases, G_c increases first, then decreases for $n > 0$, the position of the maximal value increasing from 0 as the exponent n increases from 0 (Fig. 12). The case of $n = 0$ is studied later. If the adherence is not too high, delamination can occur for a critical value of G and after the propagation of delamination can occur at constant value of this ratio. So this model provides some explanation of the main experimental feature (Fig. 8) if the observed values of y_p/c are situated in the increasing part of the curves $G(y_p/c)$. We shall verify this important point below. Notice that the delamination force F_d is also constant. The second principle induces that during delamination ($\mathrm{d}c/\mathrm{d}t > 0$):

$$G_c = w + D \quad \text{with } D \geqslant 0 \quad \Rightarrow \quad G_c \geqslant w \tag{22}$$

D is a first term of dissipation during film delamination. The second is related to the extension of the plastic deformation of the delaminated film. As y_p/c is constant, $\mathrm{d}y_p/\mathrm{d}t = (y_p/c)\,\mathrm{d}c/\mathrm{d}t$; so, after elementary calculations, one obtains from (18), by assuming $y_{ed} \ll y_p$:

$$\left(F_d - \frac{\partial V}{\partial y_p}\right) \frac{\mathrm{d}y_p}{\mathrm{d}t} = \left(2\sigma_1' h \frac{(y_p/c)^2}{1 + (y_p/c)^2} \varepsilon_p^n + \frac{2h\sigma_1'^2}{E^*} \left[\frac{1 - (y_p/c)^2}{1 + (y_p/c)^2}\right] \varepsilon_p^{2n}\right) \frac{\mathrm{d}c}{\mathrm{d}t} \tag{23}$$

Thus the work dissipated by plastic deformation par unit length (and width) of film is:

$$W_p = \sigma_1' h \frac{(y_p/c)^2}{1 + (y_p/c)^2} \varepsilon_p^n + \frac{h\sigma_1'^2}{E^*} \left[\frac{1 - (y_p/c)^2}{1 + (y_p/c)^2}\right] \varepsilon_p^{2n} \tag{24}$$

The second term is small with respect to the first.

One reports in Fig. 13 the evolution of plastic work versus the available energy release rate: it is much higher than the effective interface rupture energy and increases dramatically as G increases and tends toward its maximal value: this

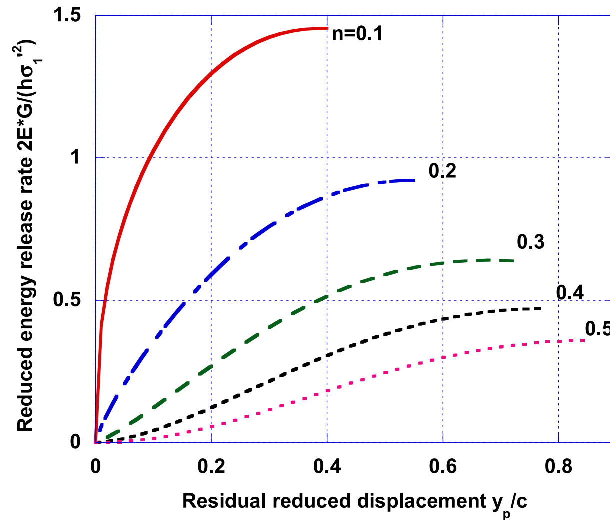

Fig. 12. Theoretical evolution of the reduced energy release rate with the residual reduced chip displacement for various values of the strain hardening exponent. One draws only the initially increasing part of the curve corresponding to stable propagation of the delamination.

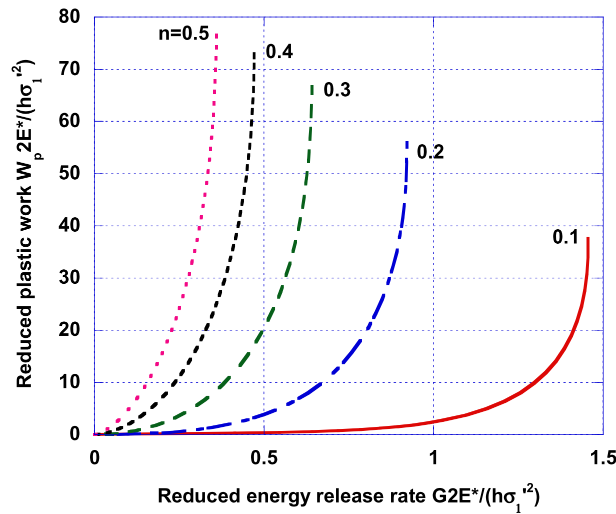

Fig. 13. Theoretical evolution of the reduced plastic work with the reduced energy release rate for various values of the strain hardening exponent ($E^*/\sigma_1' = 173$).

means that the bulk dissipated energy increases dramatically as the adhesion increases, a feature well known. For too high adhesion only plastic extension of the film till rupture occurs without any delamination.

The limit case of the elastic–perfectly plastic solid ($n = 0$) is interesting to compare. In this case, the film delamination can occur only under elastic strain without plastic strain. The elastic strain and the stress σ related to a displacement y_e are simply, by assuming $y_e \ll c$:

$$\varepsilon_e = \ln\sqrt{1 + \frac{y_e^2}{c^2}} \sim \frac{y_e^2}{2c^2}, \qquad \sigma = E^*\varepsilon_e \leqslant \sigma_1 \tag{25}$$

The inequality defines the maximal elastic strain of the film just at yielding. The variable free energy is:

$$V(y_e, c) = \frac{E^*}{2} 2ch\varepsilon_e^2 + 2wc = E^*h\frac{y_e^4}{4c^3} + 2wc \tag{26}$$

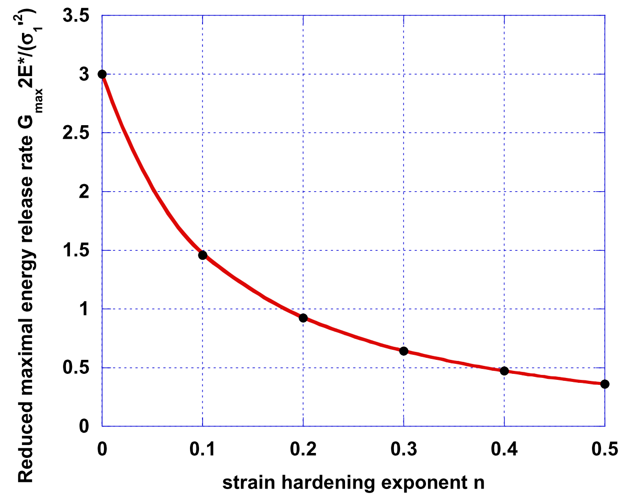

Fig. 14. Theoretical evolution of the reduced maximal energy release rate $G_{\max}$ with the strain hardening exponent of the film.

So the force F and the strain energy release rate G are:

$$\begin{cases} F = \dfrac{\partial V}{\partial y_e} = E^* h \dfrac{y_e^3}{c^3} \\ G = -\dfrac{\partial V}{2\partial c} + w = \dfrac{3}{8} E^* h \dfrac{y_e^4}{c^4} \leqslant \dfrac{3h\sigma_1'^2}{2E^*} \end{cases} \tag{27}$$

The maximal value of G is obtained as yielding occurs (cf. relations (21)). The previous relations are given by Gent with the angle (assumed small) $\theta = y_e/c$ [32]. Fig. 14 reports the evolution of the maximal energy release rate with the strain hardening exponent n: if decreases dramatically as n increases.

4.2. Mechanical properties of copper films and interpretation of CSN tests

The mechanical properties of copper thin films must be put in the model to calculate the deformation energy of the blister and the critical energy release rate. The important material parameters are the elastic modulus E and the stress–plastic strain curve $\sigma(\varepsilon_p)$.

First some brief considerations about the films. The residual stresses of copper films were measured using a commercial apparatus FLEXUS from KLA-Tencor Corp. An average tensile stress of 70 MPa was found for each sample. As CSN test lead to an important plastic deformation of the film, the influence of the residual stresses of the material (i.e. elastic work stored in the film) is assumed negligible and they are not taken into account for quantitative analysis. The work produced by tensile residual stresses is assumed to be very small compared to the energy provided by the indenter during the delamination process. Electron Back-Scattering Diffraction (EBSD) measurements on samples with processes A, B and C showed that Cu films are not textured; there is no preferred orientation of the grains. The average grain size is small compared to thickness of the film. In this article, copper is then assumed to be isotropic, and we considered that the in-plane properties are close to the through thickness properties which can be obtained by nanoindentation measurements.

Hardness and modulus of copper thin films were measured by standard nanoindentation using Continuous Stiffness Measurement (CSM) and the Oliver–Pharr procedure [34]. A sharp and well calibrated Berkovich indenter was used. The use of the Oliver–Pharr procedure to identify the mechanical properties of metallic films is debatable, as discussed previously [18,25], but our aim is to obtain orders of magnitudes in order to test our model, which is also debatable. So refinements in the interpretation of nanoindentation measurements are not performed.

The Young's modulus curves are not depicted because no significant difference was found between samples A, B and C. Modulus values also slightly increase during penetration, but it is due to the progressive influence of the stiffer substrate. The average modulus E measured between 40 nm and 80 nm of depth is 110 GPa for all the samples. So, by assuming $\upsilon = 0.35$, one has $E^* \sim 125$ GPa.

In Fig. 15 we can observe first a sharp initial decrease of hardness due to measurement errors in very small penetration depths. Then for each sample, hardness increases with penetration depth from 80 nm depth to the interface (600 nm). The values are quite stable between 30 nm and 80 nm of depth. Some differences are observed between Cu films deposited with processes A, B and C. Between 30 nm and 80 nm, average hardness H is 1.15 GPa for copper films deposited with process A, 1.07 GPa for process B and 0.8 GPa for process C (Table 1). For the stable value, one applies the Tabor's model [35] which provides a first relation between the strength and the strain hardening exponent:

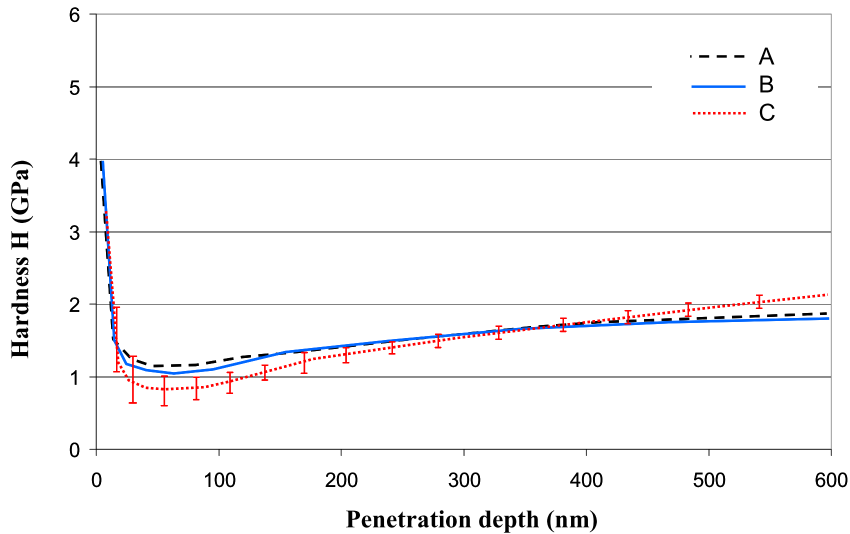

Fig. 15. Average curves of the evolution of the hardness of films A, B and C with the penetration depth.

Table 1
Evolution of the average hardness with the penetration depth of the films A, B, C and the estimated strength σ_1 and strain hardening exponent n.

Films	H_m(30–80 nm) (GPa)	H(600 nm)/H_m	σ_1 (GPa)	n
A	1.15	1.63	0.72	0.25
B	1.07	1.66	0.68	0.26
C	0.8	2.65	0.94	0.5

Table 2
Interpretation of the results of the CSN tests with the model of elastic–plastic pull-off.

Films	$y_p/c = u_f/(a-b)$	ε_p	y_{ed}/c	ε_{ed}	F_d (mN/mm)	W_p (J/m^2)	G_c (J/m^2)
A	0.144	0.01	0.0138	0.0021	49	3.54	0.49
B	0.22	0.023	0.011	0.0023	74	8.6	0.59
C	0.47	0.1	0.007	0.0027	158	37	0.64

$$\sigma(0.08) = \sigma_1(0.08)^n \approx \frac{H(30\text{–}80\ \text{nm})}{3} \tag{28}$$

One performs numerical simulation of the bilayer copper film on silicon substrate [18]. So one demonstrates that the increase of the hardness as the penetration depth increases remains low for an elastic–perfectly plastic film ($n = 0$) and is due to the growth of the pile-up around the indenter [36]. This work is described in detail in [18,25]. On the other hand, one observes a very significant increase of the hardness when indenting a strain hardening film: this effect is due to the increase of the plastic strain of the film which is progressively more and more crushed between the indenter and the much harder substrate. Thus one identifies the order of magnitude of the strain hardening of the films. Table 1 gathers the results. We see that the strain hardening of film B: $n = 0.26$ is a little higher than that of A: $n = 0.25$ whereas it is two times higher for film C: $n = 0.5$.

Table 2 gathers the results of the model applied to the films A, B and C. One assumes that for each film $y_p/c = S$. In all cases, one can apply the model because S is smaller than the reduced plastic strain related to the maximal value of the energy release rate: for $n = 0.25$: > 0.6 and for $n = 0.5$: > 0.8 (Fig. 12). One sees that the elastic displacement is much smaller than the plastic one by a factor greater than 10. Elastic strain is in all cases very small, about 0.2%. The plastic strain is greater: equal to 1% for film A, and it is about 10% for film C. One sees that all other quantities increase from films A to films C, but not with the same amplitude: The force and the plastic work increases greatly: factor 3.2 for F_d and 10 for W_p. On the contrary the critical energy release rate increases only a little: for film A: 0.49; film B: 0.59 and 0.64 J m^{-2} for film C. So the conclusions drawn from the values of S are correct, but the difference in adhesion is not so large. These values of G_c are rather low and could correspond to the Dupré's work of adhesion.

In conclusion, one must underline that it is difficult to verify in detail in these experiments the reliability of the model, because it is not easy to determine the exact geometry of the delaminated blister along the boundary of the silicon chip. One proposes in Fig. 16 to perform the CSN test on a film with a width l smaller than the blister width: this would make easier the delamination process and examination of the final geometry of the film and so would permit a better evaluation of the reliability of the present pull-off model.

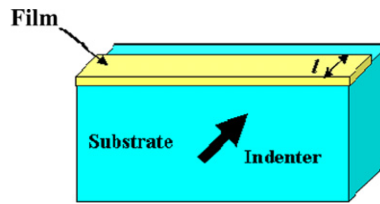

Fig. 16. Possible improvement of the CSN test by changing the geometry of the film.

5. Conclusions

CSN is a powerful technique to study the adhesion of ductile thin films on brittle substrate. No sample preparation is needed, only cross sectioning. The crack path is directly observed without specific treatment. One of the main interests of the CSN test is its ability to study local delamination on blanket and complex patterned structures, which seems impossible with other adhesion characterization techniques.

Qualitative analysis of CSN tests provides major information on the debonding behavior of copper films. Delaminated blister dimensions are strongly related to the thin film adhesion. Adhesion can be evaluated comparing the geometrical ratios S of blister dimensions.

One has proposed first a simple mechanical model of the edge chipping of the substrate which provides better agreement with experimental results than previous models. A model of pull-off of an elastic-strain hardening film which explains the proportionality between the chip displacement and the delaminated length has been developed; in addition it provides an estimation of the interface critical energy release rate. Finally, some improvements for performing CSN test in order to make easier the application of this test have been proposed.

Acknowledgements

The authors would like to thank Georges Bossis from the *Centre de micro et nano rhéometrie*, laboratoire de physique de la matière condensée, université de Nice-Sophia-Antipolis, for his support during this work. They thank very much Alchimer SA for the financial and technical support of this work.

References

[1] E. Darque-Ceretti, E. Felder, Adhésion et adhérence. Sciences et techniques de l'ingénieur, CNRS Editions, Paris, 2003, pp. 246–251.
[2] A.A. Volinsky, N.R. Moody, W.W. Gerberich, Interfacial toughness measurements for thin films on substrates, Acta Mater. 50 (2002) 441–466.
[3] G.J. Klingenmaier, M. Dobrash, in: K.L. Mittal (Ed.), Adhesion Measurement of Thin Films, Thick Films and Bulk Coatings, in: ASTM STP, vol. 640, ASTM, Philadelphia, 1978, pp. 369–390.
[4] A. Bagchi, G.E. Lucas, Z. Suo, A.G. Evans, A new procedure for measuring the decohesion energy for thin ductile films on substrate, J. Mater. Res. 9 (7) (1994) 1734–1741.
[5] A. Bosseboeuf, M. Dupeux, M. Doutry, T. Bourouina, D. Bouchier, D. Debarre, Characterization of W films on Si and SiO_2/Si substrates by X-ray diffraction, AFM and blister test adhesion measurements, Microsc. Microanal. Microstruct. 8 (1997) 261–272.
[6] R.H. Dauskardt, M. Lane, Q. Ma, N. Krishna, Adhesion and debonding of multi-layer thin film structures, Eng. Fract. Mech. 61 (1998) 141–162.
[7] Z. Gan, S.G. Mhaisalkar, Z. Chen, S. Zhang, Z. Chen, K. Prasad, Study of interfacial adhesion energy of multilayered ULSI thin film structures using four-point bending test, Surf. Coat. Technol. 198 (2005) 85–89.
[8] C.S. Litteken, R.H. Dauskardt, Adhesion of polymer thin-films and patterned lines, Int. J. Fract. 119/120 (2003) 475–485.
[9] S.S. Chiang, D.B. Marshall, A.G. Evans, A simple method for adhesion measurements, in: J.A. Pask, A.G. Evans (Eds.), Surfaces and Interfaces in Ceramics and Ceramics–Metal Systems, Plenum, New York, 1981, pp. 603–617.
[10] P.R. Jindal, D.T. Quinto, G.J. Wolfe, Adhesion measurements of chemically vapor deposited and physically vapor deposited hard coatings on WC–Co substrates, Thin Solid Films 154 (1987) 361–375.
[11] P.K. Mehrotra, D.T. Quinto, Techniques for evaluating mechanical properties of hard coatings, J. Vac. Sci. Technol. A 3 (6) (1985) 2401–2405.
[12] M.D. Drory, J.W. Hutchinson, Measurement of the adhesion of a brittle film on a ductile substrate by indentation, Proc. R. Soc. Lond. A 452 (1996) 2319–2341.
[13] A.A. Volinsky, N.I. Tymiak, M.D. Kriese, W.W. Gerberich, J.W. Hutchinson, Quantitative modeling and measurement of copper thin film adhesion, Mat. Res. Soc. Symp. Proc. 539 (1999) 277–290.
[14] A.A. Volinsky, J.B. Vella, W.W. Gerberich, Fracture toughness, adhesion and mechanical properties of low-K dielectric thin films measured by nanoindentation, Thin Solid Films 429 (2003) 201–210.
[15] J.B. Vella, S.M. Smith, A.A. Volinsky, I.S. Adhihetty, Adhesion quantification of post-CMP copper to amorphous SiN passivation by nanoindentation, Mat. Res. Soc. Symp. Proc. 649 (2001).
[16] P. Laeng, P.A. Steinmann, Adhesion testing of hard C.V.D. coatings using the scratch test, in: Proc. of the 8th Int. Conf. C.V.D., Electrochem. Soc., Pennington, 1981, pp. 723–735.
[17] E. Felder, C. Angélélis, M. Ducarroir, M. Ignat, P. Mazot, Propriétés mécaniques des films minces : Problématiques et moyens de mesure, Ann. Chim. Sci. Mat. 23 (1998) 791–819.
[18] S. Roy, Mesure de l'adhérence et des propriétés mécaniques de couches minces sub-microniques. Application aux procédés de dépôt Alchimer pour la microélectronique et au biomédical, Ph.D. Dissertation, Ecole des Mines de Paris, 2008.
[19] J. Lesage, P.H. Demarecaux, O. Bartier, G. Mesmacque, Détermination de l'adhérence de revêtements par le test d'indentation interfaciale, Rev. de Métall. – CIT 90 (12) (1993) 1655–1663.

[20] J.M. Sanchez, S. El-Mansy, B. Sun, T. Scherban, N. Fang, D. Pantuso, W. Ford, M.R. Elizalde, J.M. Martinez-Esnaola, A. Martin-Meizoso, J. Gil-Sevillano, M. Fuentes, J. Maiz, Cross-sectional nanoindentation: a new technique for thin film interfacial adhesion characterization, Acta Mater. 47 (17) (1999) 4405–4413.
[21] M.R. Elizalde, J.M. Sanchez, J.M. Martinez-Esnaola, D. Pantuso, T. Scherban, B. Sun, G. Xu, Interfacial fracture induced by cross-sectional nanoindentation in metal–ceramic thin film structures, Acta Mater. 51 (2003) 4295–4305.
[22] T. Scherban, D. Pantuso, B. Sun, S. El-Mansy, J. Xu, M.R. Elizalde, J.M. Sanchez, J.M. Martinez-Esnaola, Characterization of interconnect interfacial adhesion by cross-sectional nanoindentation, Int. J. Fract. 119/120 (2003) 421–429.
[23] J.M. Molina-Aldareguia, I. Ocaña, D. González, M.R. Elizalde, J.M. Sánchez, J.M. Martínez-Esnaola, J. Gil-Sevillano, T. Scherban, D. Pantuso, B. Sun, G. Xu, B. Miner, J. He, J. Maiz, Adhesion studies in integrated circuit interconnect structures, Eng. Fail. Anal. 14 (2) (2006) 349–354.
[24] I. Ocana, J.M. Molina-Aldareguia, D. Gonzalez, M.R. Elizalde, J.M. Sanchez, J.M. Martinez-Esnaola, J. Gil Sevillano, T. Scherban, D. Pantuso, B. Sun, G. Xu, B. Miner, J. He, J. Maiz, Fracture characterization in patterned thin films by cross-sectional nanoindentation, Acta Mater. 54 (2006) 3453–3462.
[25] S. Roy, E. Darque-Ceretti, E. Felder, H. Monchoix, Cross-sectional nanoindentation for copper adhesion characterization in blanket and patterned interconnect structures: experiments and three-dimensional FEM modeling, Int. J. Fract. 144 (2007) 21–33.
[26] H. Chai, B.R. Lawn, A universal relation for edge chipping from sharp contacts in brittle materials: A simple means of toughness evaluation, Acta Mater. 55 (2007) 2555–2561.
[27] J. Lankford, D.L. Davidson, The crack-initiation threshold in ceramic materials subject to elastic/plastic indentation, J. Mater. Sci. 14 (1979) 1662–1668.
[28] J.-I. Jang, G.M. Pharr, Influence of indenter angle on cracking in Si and Ge during nanoindentation, Acta Mater. 56 (2008) 4458–4469.
[29] B.R. Lawn, A.G. Evans, A model for crack initiation in elastic/plastic indentation fields, J. Mater. Sci. 12 (1977) 2195–2199.
[30] D.B. Marshall, B.R. Lawn, Indentation of brittle materials, in: P.J. Blau, B.R. Lawn (Eds.), Microindentation Techniques in Materials Sciences and Engineering, in: ASTM STP, vol. 889, ASTM, Philadelphia, 1986.
[31] B.R. Lawn, A.G. Marshall, Hardness, toughness and brittleness: an indentation analysis, J. Am. Ceram. Soc. 62 (1977) 347–350.
[32] A.N. Gent, New and improved tests for adhesion, J. Adhesion 23 (1987) 115–122.
[33] P. Baqué, E. Felder, J. Hyafil, Y. D'Escatha, Mise en forme des métaux. Calculs en plasticité, Dunod, Paris, 1974.
[34] W.C. Oliver, G.M. Pharr, An improved technique for determining hardness and elastic modulus using load and displacement sensing indentation experiments, J. Mater. Res. 7 (6) (1992) 1564–1583.
[35] D. Tabor, The Hardness of Metals, Clarendon Press, Oxford, 1951.
[36] D. Lebouvier, P. Gilormini, E. Felder, Theoretical and experimental study of the flow pressure and deformation of hard and soft coatings during plastic indentation, in: Proceedings of the 5th International Congress on Tribology, Eurotrib '89, Helsinki, vol. 2, 1989, pp. 116–121.